Journal of Magnetic Resonance **143,** 24–29 (2000)
doi:10.1006/jmre.1999.1959, available online at http://www.idealibrary.com on IDEAL®

Diffusion-Weighted Imaging of Bacteria Colonies in the STRAFI Plane

K. J. Carlton,[1] M. R. Halse, and J. H. Strange

The Physics Laboratory, University of Kent, Canterbury, Kent, CT2 7NR, United Kingdom

Received December 14, 1998; revised July 20, 1999

Imaging colonies of bacteria in water suspension using NMR requires that the water inside the bacteria can be differentiated from the surrounding water. This is commonly carried out by using diffusion-weighted pulsed field gradient techniques. However, it is also possible to use the diffusion sensitivity inherent in stray field imaging (STRAFI). In STRAFI, the subject to be imaged is normally moved along the axis of a superconducting magnet so that it passes through the sensitive slice. However, by moving the sample in the *transverse* direction and by using a long copper strip in place of a surface induction coil, a diffusion-weighted one-dimensional projection profile can be obtained across the sensitive slice. Profiles from a water phantom and from a bacteria suspension show convincing discrimination between intracellular and extracellular water.

Key Words: **NMR; STRAFI; diffusion-weighted imaging; bacteria; surface probe.**

INTRODUCTION

Water treatment plants routinely remove toxins from the water by passing it through a granular activated carbon filter. The toxins are adsorbed onto the surface of the carbon. Certain strains of bacteria, *biofilms*, are able to live on the carbon surface and metabolize the toxins thus extending the useful life of the filter. Paramagnetic centers commonly found on carbon filter material produce serious susceptibility line broadening of fluids in their vicinity. We have investigated the use of stray field NMR techniques (STRAFI) to detect and image bacteria colonies *in situ* at much shorter echo times than are used in conventional pulsed field gradient (PFG) experiments (*1*).

Intracellular water can be distinguished from extracellular water because of the restriction imposed on its diffusion by the bacteria cell wall. Water trapped inside the cell will show the characteristics of bounded diffusion, while water outside will be unbounded. Using this idea Potter *et al.* (*2*) employed pulsed field gradient techniques to assay cultures of bacteria and to produce a projection image of bacteria concentration using one-dimensional frequency encoding. The bacteria were placed on quartz grains which had been washed to reduce the level of paramagnetic impurities as far as possible.

[1] To whom correspondence should be addressed at present address: Canterbury Christ Church University College, Canterbury, Kent, CT1 1QU, UK. Fax: +44 (0) 1227 470442. E-mail: K.J.Carlton@canterbury.ac.uk.

Poor signal-to-noise ratios were encountered when we used this approach. It is well known that for the majority of bacteria strains, including the one used in the present experiments, the cell wall is not impervious to water (*3*) so that water is continuously exchanged between the cell interior and the outside world. If the timescale of this exchange is less than the timescale of our PFG experiments (20 ms) then the echo amplitudes will be greatly reduced.

To overcome these difficulties we have employed the STRAFI technique, after Samoilenko *et al.* (*4*). In this method the sample is located at the edge of the magnet in a position of large constant linear magnetic field gradient. This large stable "fringe field" gradient allows shorter diffusion timescales to be studied. The region of spins excited by the spectrometer, the "sensitive slice," is determined by the bandwidth of the RF pulse, (Eq. [5]). One-dimensional profiles can be obtained by moving the sample along the axis of the magnet through the sensitive slice region. Glover *et al.* (*5*) have recently used the technique to image the cross-sectional profiles of planar films. In these experiments the film is orientated so that it is coplanar with the sensitive slice. A small solenoid coil is placed adjacent to the film and the external return field from the coil is used to provide the B_1 field. The sensitive slice effectively localizes the region of excitation so that a section within the film may be investigated.

The imaging system described here is an extension of that described above. It uses a single copper strip to provide the B_1 field and exploits the effects of bounded diffusion to discriminate against the extracellular water. For the case of bounded diffusion in a large constant gradient, a spin echo will be increasingly attenuated with increasing τ. For a spherical boundary of radius R, Neuman (*6*) showed that this attenuation is given by

$$\ln\frac{M(2\tau, G)}{M_0} = -\frac{2\gamma^2G^2}{D}\sum_{m=1}^{\infty}\frac{\alpha_m^{-4}}{\alpha_m^2R^2-2}\times\left(2\tau-\frac{3-4\exp(-\alpha_m^2D\tau)+\exp(-\alpha_m^2D2\tau)}{\alpha_m^2D}\right), \quad [1]$$

where D is the diffusion coefficient of water inside the bacteria

1090-7807/00 $35.00

and G is the stray field gradient. The α_m are the roots of the equation

$$\alpha_m R J'_{3/2}(\alpha_m R) - \tfrac{1}{2} J_{3/2}(\alpha_m R) = 0, \qquad [2]$$

where $J_{3/2}$ is the Bessel function of order 3/2 and $J'_{3/2}$ is its differential. For reference, the first five values of α_m are 2.0815, 5.940, 9.206, 12.405, and 15.579.

In the free diffusion limit where $\tau \ll R^2/D$ this equation reduces to

$$\ln \frac{M(2\tau, G)}{M_0} = -\frac{2\gamma^2 G^2 D \tau^3}{3}, \qquad [3]$$

while in the limit of times long compared with the time necessary for diffusion to a boundary, i.e., when $\tau \gg R^2/D$, this equation becomes

$$\ln \frac{M(2\tau, G)}{M_0} = -\frac{R^4 \gamma^2 G^2}{D} \cdot \frac{8}{175} \cdot 2\tau. \qquad [4]$$

Thus in the presence of a strong fringe-field gradient, the signal obtained from freely diffusing water will decay rapidly as τ^3 (Eq. [3]), whereas the signal from bounded water inside the bacterium cell will decay much more slowly, proportional only to τ (Eq. [4]). For short τ the signal will be from all of the water, but at longer τ the signal from the bounded water will remain when the signal from the free water has decayed below the noise floor.

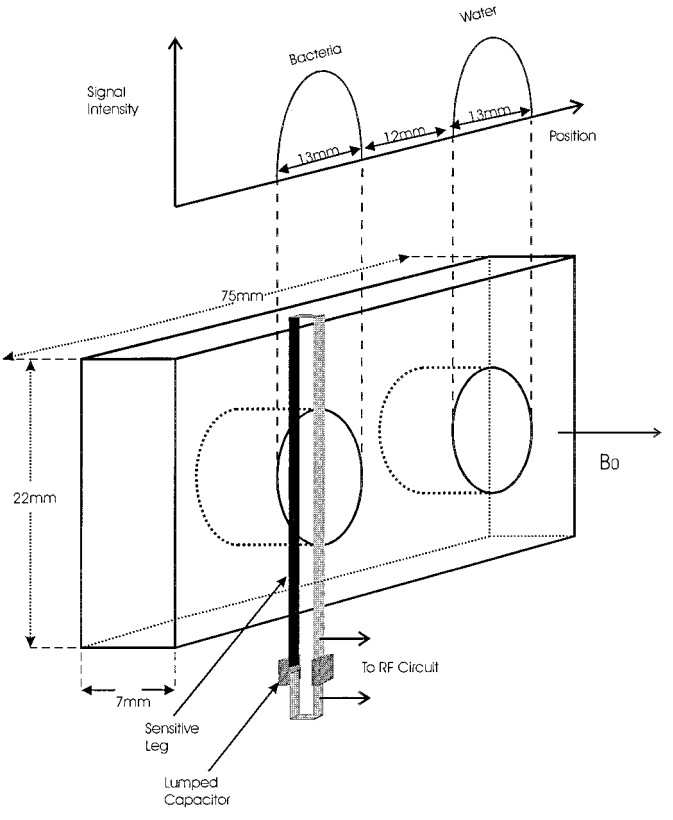

FIG. 2. Sketch showing the RF probe together with the glass sample holder used for the water and bacteria suspension phantoms. A projection profile (indicated) is obtained by moving the probe in a direction perpendicular to B_0 across the face of the sample holder.

EXPERIMENTAL

A sample of bacteria suspension was prepared by fermenting a culture of *Flavobacterium* strain P25 isolated by Mason and Burns (*7*). These bacteria are rod shaped, 1 μm in diameter, and varying in length between 1 and 2 μm, as measured under a microscope (*7*). The sample of live bacteria was concentrated after harvesting to approximately 10^{11} cells/ml using a centrifuge. The concentration of this bacteria suspension was measured using a method of successive dilution followed by a physical count using a microscope.

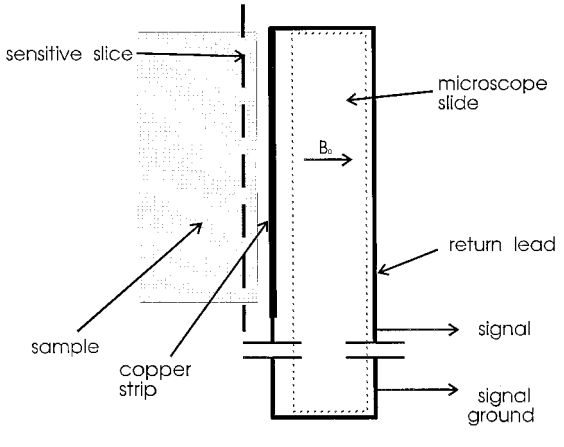

FIG. 1. Side view of the RF surface probe showing the position of the sensitive slice (vertical dashed line), the RF probe, and sample.

The STRAFI operating point was determined by measuring B_0 along the axis of our 4.7-T magnet using a Hall probe. The maximum gradient was found to be 18.3 Tm^{-1} at a point corresponding to a field of 2.5 T (107 MHz for protons). The RF surface coil, shown in Figs. 1 and 2, is designed in the shape of a thin rectangular single-turn coil placed with its axis perpendicular to the direction of the main field. The coil is made from a strip of copper sheet of thickness 0.2 mm and width 0.3 mm and is approximately 50 mm in total length. The coil is formed around a piece of glass cut from a standard microscope slide so that each leg is 25 mm long. The return leg of the coil lies behind the front leg and, since it is much further away from the sample, its effects can be ignored. The capacitors are ordinary lumped components with values chosen to resonate at the desired frequency.

As is usual in STRAFI, the spectral frequency of the RF pulse applied within the stray field gradient selects the imaged (sensitive) slice normal to the B_0 direction (*8*), as shown by the

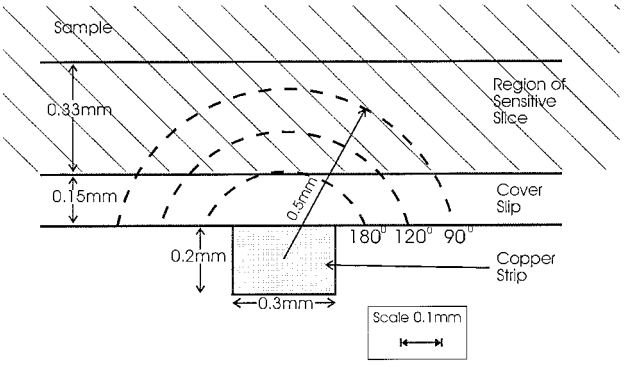

FIG. 3. Scale drawing showing the relative position for maximum signal of the RF surface probe, the phantom, and the STRAFI sensitive slice. Contours of the B_1 field strength are approximately circles centered on the center of the copper strip. The optimum 120° tip angle contour reaches approximately to the middle of the sensitive slice.

dashed line in Fig. 1. In addition, the small width of the copper strip comprising the coil, combined with its translation along the transverse axis (Fig. 2), localizes the region to a strip within this slice.

In order to produce a test image, a glass sample holder was constructed as shown in Fig. 2. One of the circular wells was filled with water and the other was filled with bacteria suspension. The samples were sealed in place by supergluing a microscope coverslip 0.15 mm in thickness over the top. The front leg of the surface probe was then placed close to the glass coverslip as shown in Figs. 1 and 3. Experiments were carried out at a temperature of 21 ± 1°C.

The RF was applied in the form of two pulses of tip angle α, each of duration $t_\alpha = 4$ μs, with a pulse separation τ varying from 40 to 1000 μs. For hard RF pulses, such a sequence has a spin-echo amplitude given by $M(2\tau) = M_0 \sin\alpha\,(\cos\alpha - 1)$ and therefore has an optimum tip angle of $\alpha = 120°$. However, this result is only approximate because phase evolution of the spins during the pulses in the large stray field gradient has been neglected. The width of the sensitive slice excited by the RF pulses is given approximately by

$$\Delta z \approx \frac{2\pi}{\gamma G_z t_\alpha}, \qquad [5]$$

which for $G_z = 18$ Tm^{-1} and $t_\alpha = 4$ μs gives $\Delta z = 0.3$ mm. Note that since the RF output could not be amplitude modulated, a conventional (90°–τ–180°–spin echo) sequence would have required pulses of different duration thus exciting different slice widths. We avoid this complication by using identical pulses. For a more detailed analysis of the spin-echo pulse sequences used in STRAFI and of accurate calculations of the echo amplitudes the reader is referred to the papers by Kimmich and Fischer (*9*) and Benson and McDonald (*10*).

To find the correct operating point, the RF current was set to a low nominal value and the whole probe assembly was moved along the axis of the magnet to locate the position of optimum signal. The amplitude of the RF current was then adjusted to give maximum signal. Figure 3 shows, to scale, the relative positions of the copper strip, the glass cover slide, the sensitive slice, and the sample at this point.

At 107 MHz, the skin depth of copper is approximately 6 μm, so that the RF current is confined to the surface of the copper strip. Numerical calculations show that the B_1 contours approximate to circles centered on the center of the copper strip. Further numerical calculations, based on the hard pulse approximation, show that maximum signal is obtained from the slice when the 120° flip angle contour extends about halfway into the slice as shown in Fig. 3. The corresponding RF current is then approximately 15 A zero-to-peak. The contribution to the signal from those parts of the sample receiving tip angles of less than 90° is estimated to be no more than about 20% of the total signal. A good estimate of the in-plane resolution of the probe can therefore be found by observing the horizontal distances (±0.43 mm) where the 90° contour leaves the sample. We therefore expect the in-plane resolution to be approximately 0.9 mm and the signal to originate from a sensitive region of order 0.3 × 0.9 × 25 mm.

RESULTS

The images produced are shown in Fig. 4. At each position of the copper probe the signal was acquired for 100 averages with a repetition time of 1 s. This was repeated at 45 positions as the probe was moved across the sample in 1-mm steps. The total imaging time for each profile was therefore a little over 1 h. Figure 4a shows the one-dimensional profiles of the water and bacteria suspension produced with $\tau = 40$ μs (diamond data points).

The profiles are nonideal for several reasons. The amplitude of the signal from the bacteria suspension is less than that from the water. This cannot be accounted for by T_2 effects because the short echo time $2\tau = 80$ μs is much less than the T_2 of either the bacteria suspension (~8 ms) or the water. However, because of trapped air bubbles in the bacteria suspension it was not possible to ensure equal sample volumes. The flat top to the profile of the bacteria suspension in Fig. 4a is thought to be due to a ring of superglue on the microscope coverslip. In the water profile there is an additional distortion due to the presence of a large air bubble.

When the value of τ is increased to 1000 μs, as represented by the squares, the signal from the bacteria suspension is much reduced. The signal from the freely diffusing extracellular water has decayed away leaving only the signal from the intracellular water. Similarly the signal from the pure water has also decayed away due to diffusion. Finally, the superglue signal has also disappeared into the noise because of its short T_2. The resulting image is that of the water bounded by the bacteria cells. Figure 4b shows the 1000-μs profile on an

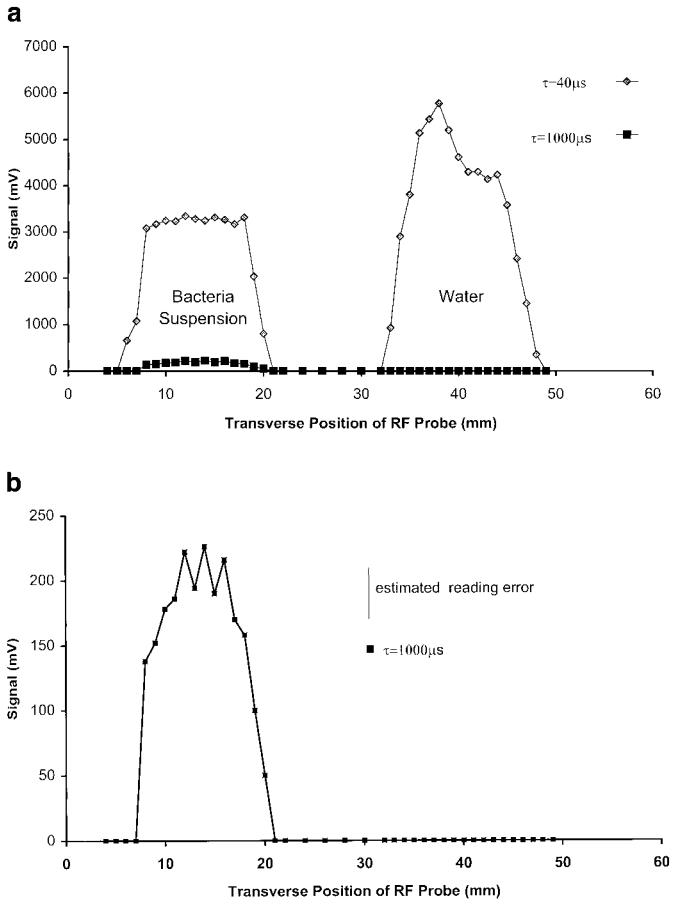

FIG. 4. One-dimensional profiles of bacteria suspension (left) and water (right) taken at $\tau = 40$ and 1000 μs. At 40 μs there is a strong signal from both the bacteria suspension and the water samples. However at 1000 μs the signal from the water in both samples is no longer visible. The voxel size for each point in the profile is approximately $0.3 \times 0.9 \times 25$ mm (see text). (b) One-dimensional profiles of bacteria suspension (left) and water (right) taken at $\tau = 1000$ μs, as in (a), but with enlarged vertical scale. At this value of τ the signal which remains comes only from the bacteria and not from the free water.

expanded scale. The bacteria profile is now closer to that expected from a cylinder. The estimated reading error quoted in Fig. 4b is the amplitude of the noise signal at the peak of the echo. The signal-to-noise ratio is approximately 10:1 for 10^{11} cells/ml. This figure is similar to that obtained by Potter *et al.* (*2*) (signal-to-noise = 4:1 for 2×10^{10} cells/ml).

FURTHER EXPERIMENTS

The long-term aim of this work is to investigate the possibility of imaging bacteria adsorbed onto GAC in a commercial water filter. In order to gain some insight into the feasibility of such experiments and to obtain useful additional information concerning bacteria concentration some additional experiments were carried out in which the RF surface probe was positioned directly over the center of the circular glass well containing the bacteria suspension and the echo amplitude $M(2\tau)$ was measured as a function of the interpulse gap τ. Measurements were performed on two bacteria suspensions: the original sample used in the profile experiments (Fig. 4) and a second sample designed to simulate a bacteria suspension as found in a commercial water filter. This second sample was made by vigorously mixing some of the original bacteria suspension using a spatula with an excess of oven-dried activated carbon. The resulting dry paste contained approximately 10% by volume of bacteria suspension.

RESULTS

Normalized plots of $\log_e\{M(2\tau)/M(0)\}$ for the original bacteria suspension and the bacteria–carbon paste are shown in Figs. 5a and 5b, respectively. For times up to ~0.5 ms the slope of both curves becomes increasingly negative followed by a less rapid decay linear in τ. The first part of each curve is identified with the freely diffusing extracellular water (the τ^3 term in Eq. [3]), while the linear part of each plot is characteristic of the bounded diffusion of intracellular water within the bacterium (Eq. [4]). The most striking feature of the results is that the slope of Fig. 5b is *less* than that of Fig. 5a. The differing effects of diffusion in the extracellular and intracellular water can be well approximated by a linear combination of Eqs. [3] and [4] to give the equation

$$M(2\tau) = (1 - A)\exp\left(-\frac{2\gamma^2 G^2 D_{\text{ext}}\tau^3}{3}\right) + A\exp\left(-\frac{R^4\gamma^2 G^2}{D_{\text{int}}}\cdot\frac{8}{175}\cdot 2\tau\right), \qquad [6]$$

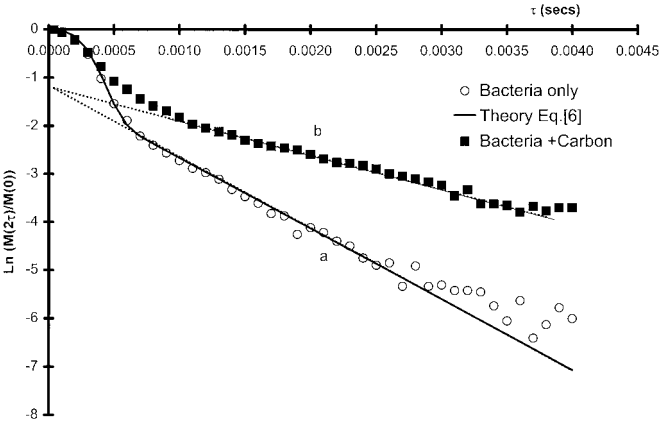

FIG. 5. Graphs of $\log_e\{M(2\tau)/M(0)\}$ versus τ for (a) bacteria suspension (open circles) and (b) a mixture of bacteria and carbon (closed squares). The initial parts of the curves show the unbounded diffusion of the intracellular and extracellular water. At echo times 2τ greater than approximately R^2/D_{int}, the diffusion of the intracellular water becomes bounded, the signal from the extracellular water is quickly lost, and the plot becomes linear in τ. The continuous line is a theoretical fit using Eqs. [1] and [6] as discussed in the text.

where A is the proportion of intracellular water, D_{int} is the diffusion coefficient of the intracellular water, D_{ext} is the diffusion coefficient of the extracellular water, and R is the mean bacteria radius. Extrapolation of the linear sections of Figs. 5a and 5b back to $\tau = 0$ both give $A = 0.26 \pm 0.02$. Thus the ratio of bacteria to nutrient solution is the same in the two samples, as expected. [*Note.* the *absolute* number of bacteria cells per milliliter in the bacteria–carbon sample was about a factor of 10 less than in the sample of Fig. 5a. This is reflected in the relative displacement of the noise floors in Figs. 5a and 5b.]

As shown by the second term of Eq. [6], the gradient of the linear section is proportional to R^4G^2/D_{int}. Although no definitive value for D_{int} is available it is reasonable to assume that it lies between 10 and 100% of that of pure water, i.e., (0.2–2.3) $\times 10^{-9}$ m^{2}s^{-1}. Since $G = 18.3$ Tm^{-1}, the gradients give $R = 0.85 \pm 0.25$ μm for the bacteria suspension (Fig. 5a) and $R = 0.7 \pm 0.2$ μm for the bacteria–carbon mixture (Fig. 5b). These dimensions are in good agreement with those quoted in Ref. (*7*). The 20% decrease in mean radius obtained in the bacteria–carbon mixture is consistent with a loss of water to the very dry carbon.

The effects of exchange between the intracellular and extracellular water can be included by multiplying the second term in Eq. [6] by a factor $\exp(-2\tau/T_{ex})$, where T_{ex} is the exchange time constant. When the bacteria are surrounded by dry carbon and the nutrient solution is adsorbed on the carbon, the exchange of water might be severely inhibited, so the exchange would affect the slope of Fig. 5a more than that of Fig. 5b. Assuming a value for T_{ex} of order 20 ms (based on our PFG experiments), the increase in gradient of the linear portion of Fig. 5a is only about 8% and therefore is easily masked by a 2% uncertainty in R. Without an independent measurement of R, it is impossible to separate out these effects.

The change in slope between Figs. 5a and 5b could be due to a number of other reasons:

(i) A decrease in D_{int} due to dehydration,

(ii) a change in the T_2 of the intracellular water due to dehydration,

(iii) an increase in susceptibility effects from paramagnetic centres in the activated carbon. It is well known that susceptibility differences can cause large local internal gradients of order $B0\Delta\chi/d$, where d is a typical pore size (*11*). Even if it is assumed that a typical pore size in the activated carbon is only 10 μm and that $\Delta\chi \approx 10^{-5}$, then with $B_0 = 2$ T, the internal gradients would be of order 2 Tm^{-1} and therefore small compared to the STRAFI gradient of 18.3 Tm^{-1}.

However in all three cases the effect would be to increase the slope as carbon is added, not decrease it as is observed.

The constant A is directly related to the bacteria concentration. Assuming bacteria of mean radius R, the cell count is $A \times 10^{-6}/\frac{4}{3}\pi R^3$ cells/ml. With $R = 0.85 \pm 0.25$ μm and $A = 0.26 \pm 0.02$, this corresponds to a figure of between 5×10^{10} and 3×10^{11} cells/ml. The uncertainty is mainly due to our lack of knowledge of D_{int} although it is not inconsistent with the direct count of 10^{11} cells/ml.

Analysis of the early part of Fig. 5a shows a τ^3 dependence indicative of free diffusion. Referring to the first term in Eq. [6] gives $D_{ext} = 1.2 \times 10^{-9}$ m^{2}s^{-1}. The overall fit using Eq. [6] (or more accurately Eq. [1]) with $D_{ext} = 1.2 \times 10^{-9}$ m^{2}s^{-1}, $R^4/D_{int} = 6.8 \times 10^{-16}$ m^{2}s, and $A = 0.26$ is shown by the continuous line in Fig. 5a. In the case of Fig. 5b, the early part of the curve varies more slowly than τ^3. This indicates that the extracellular water is not diffusing freely and no estimate of D_{ext} was possible.

The value obtained for $D_{ext} = 1.2 \times 10^{-9}$ m^{2}s^{-1} for the bacteria suspension is significantly less than that of pure unconfined water which, under the same experimental conditions, was measured to be 2.3×10^{-9} m^{2}s^{-1} in agreement with the accepted value. This surprising result could be due to an increase in the viscosity of the extracellular water caused by the presence of extracellular polymeric substance secreted by the bacteria. However even in polysaccharide gels, for example, D is typically 95% that of free water. Another possible reason for the low value of D_{ext} is a tortuosity factor, estimated to be 0.85, caused by the presence of the bacteria at these relatively large concentrations. However these two effects are unlikely to account for such a low value. At this stage no satisfactory explanation has been found. Apart from this discrepancy, the results are in good agreement with expectations. From Fig. 5a, it is estimated that the signals from the bacteria and from the water are comparable at $\tau = 500$ μs and support the choice of $\tau = 1000$ μs for the imaging experiment, Fig. 4b. From the noise floor in Fig. 5a it is estimated that the signal-to-noise ratio at $\tau = 1000$ μs is approximately 25:1. This figure is better than the 10:1 obtained for the imaging experiment because the sample remains stationary throughout. The figure corresponds to a detection limit of 4×10^9 cells/ml. Although this is at the upper end of the typical value for the concentration of bacteria in GAC and soil (about 10^9 cells/g) (*12*), it shows that, with improvements, the STRAFI technique may be applicable to a real situation.

CONCLUSIONS

The new surface probe technique allows one-dimensional transverse projection profiles to be obtained across the STRAFI sensitive slice. The in-plane resolution is limited by the dimensions of the probe and was of the order of 1 mm in these experiments. By rotating the sample between successive profiles, it should be possible to produce two-dimensional images of bacteria concentration using standard back-projection techniques. We have been able to detect bacteria in concentrations down to approximately 4×10^9 cells/ml, even in the presence of significant quantities of paramagnetic impurities such as those found in activated carbon.

ACKNOWLEDGMENT

The authors acknowledge the helpful suggestions from the referees.

REFERENCES

1. J. J. Neil, Measurement of water motion (apparent diffusion) in biological systems, *Concepts Magn. Reson.* **9**(6), 385–401 (1997).
2. K. Potter, R. L. Kleinberg, F. J. Brockman, and E. W. McFarland, Assay for bacteria in porous media by diffusion-weighted NMR, *J. Magn. Reson. B* **113,** 9–15 (1996).
3. R. Y. Stanier, J. L. Ingraham, M. L. Wheelis, and P. R. Painter, "General Microbiology," 5th ed., p. 197, Macmillan Education, London. (1987).
4. A. A. Samoilenko, D. Y. Artemov, and L. A. Sibel'dina, Formation of sensitive layer in experiments on NMR subsurface imaging of solids, *JETP Lett.* **47,** 417 (1988).
5. P. M. Glover, P. J. McDonald, and B. J. Newling, Stray-field imaging of planar films using a novel surface coil, *J. Magn. Reson.* **126,** 207–212 (1997).
6. C. H. Neuman, Spin echo of spins diffusing in a bounded medium, *J. Chem. Phys.* **60**(11), 4508 (1974).
7. J. Mason and R. G. Burns, Production of a monoclonal-antibody specific for a Flavobacterium species isolated from soil, *FEMS Microbiol. Ecol.* **73,** 4299–4307 (1990).
8. P. J. McDonald and B. Newling, Stray field magnetic resonance imaging, *Rep. Progr. Phys.* **61**(11), 1441–1493 (1998).
9. R. Kimmich and E. Fischer, One- and two-dimensional pulse sequences for diffusion experiments in the fringe field of superconducting magnets, *J. Magn. Reson. A* **106,** 229–235 (1994).
10. T. B. Benson and P. J. McDonald, Profile amplitude modulation in stray-field magnetic-resonance imaging, *J. Magn. Reson. A* **112,** 17–23 (1995).
11. S. Bahceli, A. R. S. Al-Kaisi, K. Krynicki, and J. H. Strange, The effects of pore and particle geometry on NMR diffusion measurements in adsorbed liquids, *in* "Characterisation of Porous Solids II" (F. Rodriguez-Reninoso, *et al.,* Eds.), pp. 293–300, Elsevier Science, Amsterdam (1991).
12. R. E. White, "Introduction to the Principles and Practice of Soil Science," 2nd ed., Blackwell Sci., Oxford (1979).